Synchrotron Radiolysis and Mass Spectrometry: A New Approach to Research on the Actin Cytoskeleton

JING-QU GUAN,[‡,§] STEVEN C. ALMO,[‡,¶] AND MARK R. CHANCE*[,‡,§,¶]

Center for Synchrotron Biosciences, Department of Physiology & Biophysics, and Department of Biochemistry, Albert Einstein College of Medicine, 1300 Morris Park Avenue, Bronx, New York 10461

Received October 6, 2003

ABSTRACT

Hydroxyl radicals generated from millisecond exposure of aqueous solutions to synchrotron X-rays react with proteins to yield stable oxidative modifications of solvent-accessible amino acid side chains. Following proteolysis, HPLC/MS analysis is performed to quantitate the side chain reactivities, and MS/MS analysis is used to identify the modification site(s). Side chain reactivity is shown to be correlated with solvent accessibility; thus the method provides detailed site-specific information about protein structure. The application of these techniques to the study of the actin cytoskeleton is described in detail, including defining the binding sites of monomeric actin with gelsolin segment-1, the actin monomer binding surface on cofilin, the divalent cation-dependent structure changes of monomeric actin, and the conformational changes associated with actin filamentous assembly.

Introduction

In eukaryotic cells, filamentous actin structures modulate cell morphology and control essential cellular processes including locomotion, vesicle transport, and cytokinesis.[1,2] Spatial and temporal control of these dynamic events is accomplished by actin binding proteins that change the structure of the cytoskeleton. The mechanisms by which these proteins regulate the available pool of both monomeric (G-) and filamentous (F-) actin include monomer sequestration, filament capping, filament severing, filament disassembly, and filament nucleation (Figure 1). The actin-monomer-binding protein profilin, with help in vertebrate cells from thymosin β4, maintains a pool of unpolymerized ATP−actin subunits.[3−5] In addition to G-actin sequestration, control of actin polymerization is regulated by proteins such as CapZ, which binds to and caps the barbed ends of filaments.[6] The cofilin and gelsolin families of actin regulatory proteins can bind to both G- and F-actin and display multiple functions of capping and severing actin.[7,8] The mode of cofilin binding to actin monomers is not known. The Arp2/3 complex is an assembly of seven proteins that promotes de novo nucleation of actin filaments and directs the formation of branched dendritic networks.[2] The polymerization of actin mediated through the activity of these actin binding proteins is highly dependent upon the presence of bound nucleotide and divalent cations, as well as other solution conditions.[9−15] Although many actin binding proteins are amenable to crystallographic analysis, many of the relevant functional states or higher order complexes are refractory to 3-D structure determination. In particular, due to the tendency of G-actin to polymerize, the determination of the three-dimensional structure of isolated actin monomers has been difficult because of the concentration requirements typical for X-ray crystallography and NMR approaches. In this article, we detail the development of hydroxyl radical mediated footprinting approaches to better understand the structure of these functional states.

A high-resolution structure of ADP−actin (covalently modified at Cys-374) is available,[16] and the structure of actin monomers has been analyzed in the context of their complexes with various actin binding proteins.[17−21] Actin possesses a small domain composed of subdomains 1 and 2 and a large domain composed of subdomains 3 and 4 (Figure 2a). Divalent cation bound nucleotide is coordinated deep within the cleft formed by the large and small domains.[21] Actin binding proteins such as DNase-I bind to the highly flexible "D-loop" on subdomain 2,[17] while gelsolin segment-1 and profilin bind in the cleft formed between subdomains 1 and 3.[18,19] The significant conformational flexibility of actin and its complexes demands techniques to examine its structure in detail in the solution state. Radiolytic protein footprinting approaches are well suited to addressing these questions.

The problem of structure determination for filamentous actin, due to the size and heterogeneity of the samples, is much greater than that for G-actin. Nevertheless, great strides have been made toward an atomic-level description of F-actin by fitting the atomic structure of G-actin to moderate resolution (8 Å) X-ray fiber diffraction data.[22,23] These studies have led to a helical model for the structure of F-actin, in which subsequent monomers are rotated by ∼167° and translated by 27.5 Å. This structure

Jing-Qu Guan received his Ph.D. in Chemistry from the Chinese Academy of Sciences in 1998, under the supervision of Chen-Ho Tung. After a Humboldt research fellowship at Munich University, he became a postdoctoral fellow with Mark Chance at the Albert Einstein College of Medicine in 2000. He has been a faculty member in the Department of Physiology & Biophysics since 2002. His research focus is on the applications of mass spectrometry to structural biology.

Steven Almo received his Ph.D. in Biophysics from Harvard University in 1990, while working with Gregory A. Pesko at MIT. After postdoctoral work at Johns Hopkins University with Tom Pollard and Ed Lattman, he joined the Biochemistry department at the Albert Einstein College of Medicine in 1992. He is currently Professor of Biochemistry and Physiology & Biophysics.

Mark Chance received his Ph.D. in Biophysics from the University of Pennsylvania in 1986 working with Linda Powers and Britton Chance. After postdoctoral work at the AT&T Bell Laboratories with Joel Friedman, he became Assistant Professor of Chemistry at Georgetown University in 1988. In 1992, he moved to the Albert Einstein College of Medicine and is currently Professor of Physiology & Biophysics and Biochemistry. Since 1995 he has been Director of the Albert Einstein Center for Synchrotron Biosciences, which has focused on the development and application of synchrotron radiation methods to understand the structure and dynamics of macromolecules.

* To whom correspondence should be addressed. E-mail: mrc@aecom.yu.edu. Tel: (718)430-4136.

‡ Center for Synchrotron Biosciences.

§ Department of Physiology & Biophysics.

¶ Department of Biochemistry.

10.1021/ar0302235 CCC: $27.50
Published on Web 01/23/2004

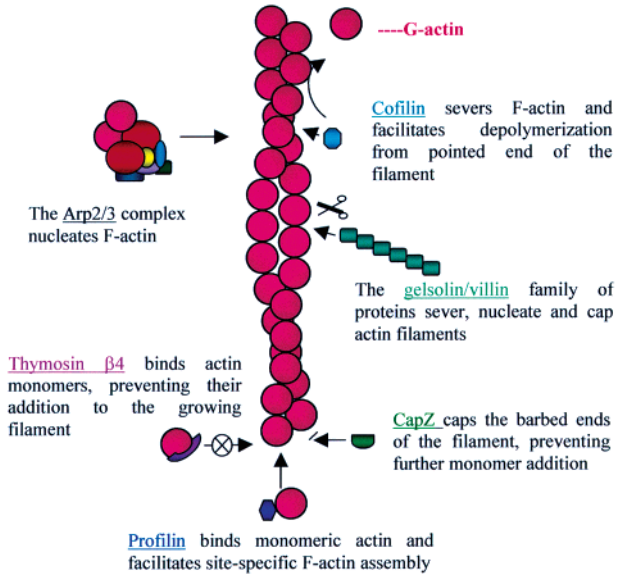

FIGURE 1. The regulation of actin filament assembly/disassembly by actin binding proteins. The combined activities of the actin binding proteins as well as divalent cation and nucleotide control actin dynamics in a highly regulated fashion.

is illustrated in Figure 2b (left), where five actin monomers are individually colored to illustrate the interactions of the monomers that give rise to the filament structure.[17,22−24] This arrangement results in one face of each of the disk-shaped actin monomers pointing towards the filament axis (inner face) with the other (outer face) facing the solvent. This results in numerous "longitudinal" contacts of the edges of the actin molecule as illustrated in Figure 2. Within Figure 2b, the actin monomer colored in purple provides the longitudinal contacts colored in blue, while the actin monomer colored in green provides the other side of the contacts colored in brown. Specifically, residues 322−325 of subdomain 3 of one monomer (Figure 2b, left, blue) are predicted to make contact with residues 243−245 in subdomain 4 of a second monomer (brown), while residues 286−289 in subdomain 3 (blue) interact with residues 202−204 in subdomain 4 (brown). In addition, residues 166−169 in subdomain 3 (blue) and residue 375 in subdomain 1 (blue) contact residues 41−45 within the D-loop of subdomain 2 (brown).[22] Lateral contacts between the filament, stabilizing the opposing strands, are proposed to be mediated by a hydrophobic "plug" (the H-loop, colored in red, Figure 2b) composed of residues 264−273.[22] This model of the actin filament is in general agreement with electron microscopy data, which suggest the importance of subdomains 1 and 2 and the C-terminus in the longitudinal contacts.[25,26] An alternative model of the actin filament was constructed using a profilin/β-actin complex, where the structure of filaments resembles a ribbon (Figure 2b, right).[27] The patterns of actin monomer interactions in the filament assemblies for these two structural models of F-actin are very different; for example, residues 260−270 are significantly buried in the helical model, whereas they are as exposed as in G-actin for the ribbon model. Since footprinting approaches are not intrinsically size-limited, their measures of side chain

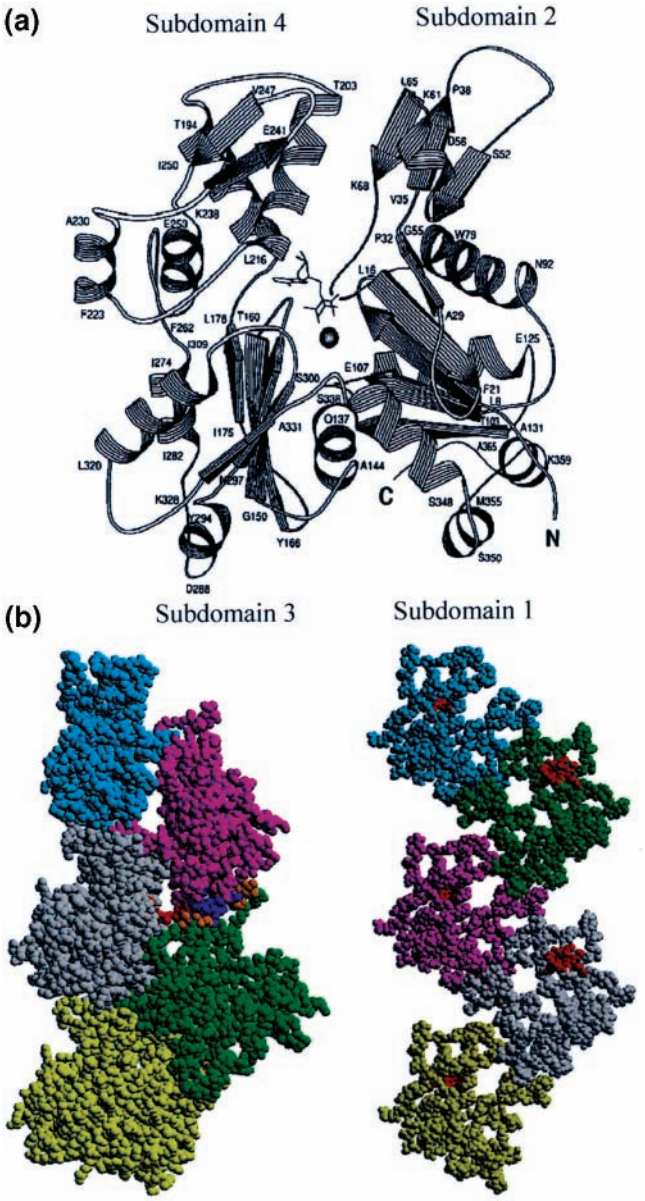

FIGURE 2. The structure of G-actin (a) and the helical (b, left) and ribbon (b, right) models for the structure of F-actin. The H-loop peptide (260−270) is colored red in both models. The longitudinal contacts are colored in brown and blue for the helical model (see text).

solvent accessibility provide valuable probes of actin filament dynamics for the study of actin's interactions with its binding proteins.

Hydroxyl radical mediated footprinting using synchrotron radiation measures changes in accessible surface areas of discrete macromolecular moieties by examining the kinetics of the reaction of those moieties with •OH generated by radiolysis. The method is especially valuable in bridging the gap between high-resolution crystallography and NMR approaches and medium to lower resolution modeling and EM methodologies, providing information on the structures of macromolecules in solution. In this Account, we describe our use of hydroxyl radical mediated footprinting with quantitative LC-coupled mass spectrometric analysis and tandem MS, for

examining the structure, function, and regulation of the actin cytoskeleton.

Radiolysis Chemistry and Reactive Oxygen-Mediated Protein Oxidation

The radiolysis of water is an effective method for generating hydroxyl radicals.[28] Interaction of photons with water (at 55 M concentration) generates a water ion and an electron within nanoseconds, and the water ion further reacts with another water molecule to yield •OH, a hydronium ion, and a "hydrated" electron (eq 1).[28] These

$$H_2O \xrightarrow{h\gamma} H_2O^+ + e^-_{dry} \xrightarrow{H_2O} H_3O^+ + {}^{\bullet}OH + e^-_{aq} \quad (1)$$

electrons and the water ions are responsible for all subsequent radiation chemistry in dilute aqueous solutions. An unfocused "white beam" bending magnet beamline at the National Synchrotron Light Source (NSLS) provides an intense X-ray source for radiolysis.[29−32]

The oxidative modification of peptides and proteins has been exhaustively studied, and the expected radiolysis products for amino acids, peptides, and proteins in dilute aqueous solution include (a) cleavage of peptide bonds, (b) cross-linking of molecular species, and (c) oxidation of amino acid residue side chains.[33,34] Cleavage results from hydroxyl radical abstraction of backbone $C_\alpha-H$ bonds, which leaves a C_α-centered radical that can react with oxygen.[35] However, hydroxyl radicals react preferentially with the side chains of amino acid residues due to the steric hindrance of main chain α-carbon under typical radiolysis conditions. Oxidation is preferred at sites where the radical will be stabilized by neighboring unsaturated bonds or electron-rich heteroatoms through electron delocalization. Thus, oxidation at aromatic and sulfur-containing amino acid residues is preferred.[35,36] Since it requires the properly oriented bimolecular association of radicals on separate macromolecules, cross-linking can be minimized in synchrotron experiments by limiting the exposure time. Thus, conditions can be easily optimized to provide primarily side chain oxidation.

Mass Spectrometry: Analyzing Radiolysis Products of Peptides and Proteins

Gentle ionizations of large biomacromolecules by electrospray (ESI) and matrix-assisted laser desorption ionization (MALDI) have become powerful tools in peptide and protein analysis.[37,38] Because the addition of a single oxygen atom to an amino acid in peptides results in stable mass increases of 16 (forming alcohols) and of 14 (forming carbonyl groups), the mass peaks of oxidized and unoxidized peptide products can be well resolved using these modern techniques.[36] The relative abundance of the oxidized and unoxidized species, and thus the extent of modification, is directly quantitated from the mass spectrometry data. To locate the oxidation site for a particular oxidized peptide, a tandem MS (MS/MS) fragmentation experiment for the peptide of interest identifies the modified side chain residue.[36−38]

To verify that the oxidation products predicted from previous metal-catalyzed and radiolytic oxidation studies are appropriate for interpreting footprinting data and to understand the range of side chains that are likely to be probed in typical experiments, detailed studies on the oxidation of peptides have been carried out.[36,39] Exposure of peptides at micromolar concentrations to a synchrotron white beam revealed substantial oxidation within tens of milliseconds and a first-order decay of the fraction of unmodified peptide, as quantitated by both MALDI/TOF and ESI mass spectrometry.[36] This supports previous experiments on nucleic acids that have indicated a constant concentration of hydroxyl radicals during the X-ray exposure.[30,32] Thus, the bimolecular association of radicals with macromolecules can be approximated as a pseudo-first-order reaction. Tandem MS experiments on the oxidized peptides demonstrated that single or multiple sites of oxidation could be explicitly identified to confirm the specific side chain probe sites.[31,36,40,41] Comparisons of the oxidation rates of different peptides revealed that the relative rate of oxidation of various side chains paralleled those expected from previous pulse-radiolysis studies and a reactivity order of Met, Cys ≫ Phe, Tyr > Trp > Pro > His, Leu was observed.[36] In the subsequent protein studies, these eight residues have shown to be excellent probes for the method.[40−45] Recent experiments have shown that a careful examination of the radiolysis chemistry can expand the relevant probe set as well.[39]

These studies on peptides suggested the feasibility of using the modification of amino acid side chains as an approach to probe protein structure in solution, as has been developed for a number of modification approaches for both protein and nucleic acid footprinting.[46,47] Specifically, proteins of interest are exposed to synchrotron X-rays for a series of exposure times, followed by proteolysis using site-specific proteases to generate defined peptide species. Coupled HPLC−MS is used to separate the peptide mixture, and the peaks corresponding to the modified and unmodified individual peptides in the total ion chromatogram are extracted (Figure 3) and compared to give the oxidation extent, that is, the fraction unmodified (the ratio of the peak area of the unmodified peptide to the sum of the peak areas from the modified and unmodified peptides). Plotting the unmodified fractions versus X-ray exposure times gives a dose response curve, which is fit as a first-order kinetics process to provide the modification rate (Figure 4).[40,45]

Modification rates explicitly reveal the reactivity of side chains of a peptide within the protein structure; however, they do not provide any information about the specific residue(s) that are oxidized in the peptide. To identify the oxidation sites (as well as to confirm the identity of the peptide in question), MS/MS is always performed after MS analysis.[40,45,48] A representative collision-induced dissociation (CID) MS/MS spectrum is shown in Figure 5a for residues 83−96 (IVFFTWSPDTAPVR) of cofilin.[45] Daughter ions of y-type (which retain charge on the C-terminus) like y_3, y_7, y_8, y_9, y_{10}, y_{11}, and y_{12} ions, and b-type ions (which retain charge on the N-terminus), like b_{13}, b_{11}, b_{10},

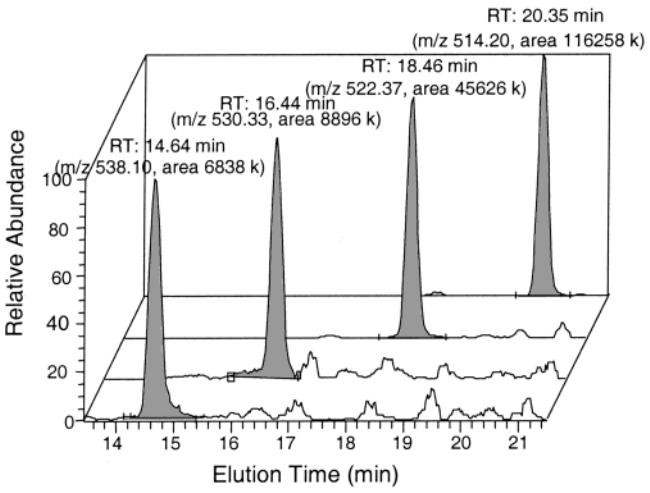

FIGURE 3. Representative extracted ion chromatograms from the total ion chromatogram used to quantitate modification extent of peptides in LC/MS. Chromatograms are shown for unoxidized and oxidized doubly charged peptide ions from residues 118−125 of actin from the 50 ms exposure of the Mg-G-actin/GS1 complex. The unoxidized species is seen at 20.35 min with an integrated area of 116 258. The singly oxidized, doubly oxidized, and triply oxidized ions are also shown. Each plot was normalized to the largest peak, the integrated area of which was used to calculate the fraction unmodified for this exposure time.

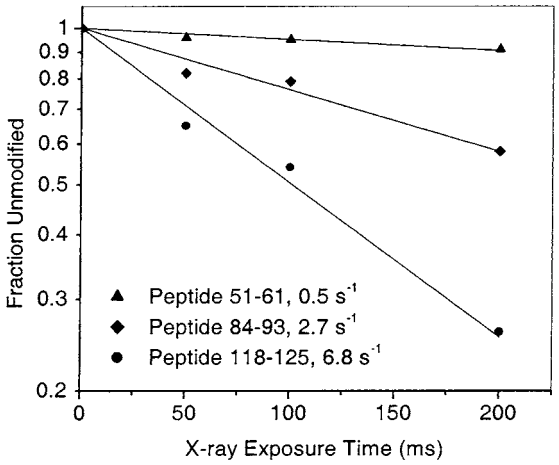

FIGURE 4. Dose response plots indicate the relative reactivities of peptides 51−61, 84−93, and 118−125 of actin in the Mg-G-actin/GS1 complex.

b_9, b_7, b_6, b_5, and b_3, are readily identified in this spectrum. When the same analysis is conducted on the singly oxidized peptide, which in this case has a mass shift of +16 relative to the parent, retention of mass on a particular daughter ion indicates that the daughter ion retains the site of modification. For example, the b_3, b_5, b_6, b_7, and b_{11} ion fragments of this peptide are unshifted relative to those in Figure 5a (b_9 and b_{10} are not observed) (Figure 5b). This suggests that oxidation takes place on the C-terminal segment PVR. Although b_{12} is not observed, b_{13} is observed as shifted by +16; thus, the site of modification is indicated to be either Pro or Val. An examination of the y-series ions indicates that for all y-series ions observed, all are shifted by mass units +16. The observation of a y_3 ion shifted by +16 is consistent with the assignment of either Val or Pro as the oxidized residue. Due to the higher reactivity of Pro than Val, Pro-94 is considered the primary probe site in this peptide.[47]

Correlation between Solvent Accessibility and Reactivity of Side Chains

The absolute rate of modification for a particular peptide depends on three factors: (1) the identity of the side chain, which determines its intrinsic reactivity (we will not deal here with context specific reactivity effects, e.g., sequence and structure, other than solvent accessibility); (2) the number of residues within the peptide; (3) the solvent accessibility of the side chain residues. It is intuitively obvious and a fundamental tenet of footprinting approaches that the reactivity of a susceptible site correlates closely with accessibility at that site.[49] For a single type of side chain within a peptide, the rate of modification should increase with increased solvent accessibility. This hypothesis is directly put to the test by examining the oxidation rate of five leucines within the structure of cofilin (Figure 6). These leucines vary considerably in solvent accessibility (from 0.2 to 120 Å^2), as calculated from the crystal structure,[50] and the observed rates of oxidation monotonically increase as the solvent accessibility increases (although not proportionally).[45] For a peptide with multiple reactive residues, a complex sum of the reactivity of the residues, their accessibility, and their number determines the modification rate; however, since the modification rate is very precisely measured, even modest changes in accessibility for one or several residues can be detected by the method.

Protein Footprinting of the Gelsolin Segment-1 Actin Complex

Solvent accessibility changes for a side chain, resulting from either allosteric conformational changes due to ligand-binding or specific protections within the protein−ligand interface, can be reflected in changes in observed rates of modification. The first validation of this method, involving the protection of a side chain residue within a binding interface, was upon examination of gelsolin segment-1 (GS1) binding to actin,[48] where the crystal structure (and subsequent footprinting experiments) of the complex indicated complete burial of GS1 residue Phe-104 upon complex formation.[18] Since this initial validation of the method, the approach has been used to study the unfolding of apomyoglobin,[41] the interactions of cofilin with actin,[45] the interactions of DNA with the TATA binding protein,[44] the divalent cation induced conformational changes of gelsolin and actin,[42,51,52] and the interacting surfaces of transferrin and transferrin receptor.[43] Throughout the development of the method, a consistency between crystallographic structural data and experimental results has been observed, as the residues predicted to be accessible are found to be modifiable while those that are buried are not.[40,43−45]

Three features of radiolytic footprinting as developed in this laboratory ensure that the intact population of

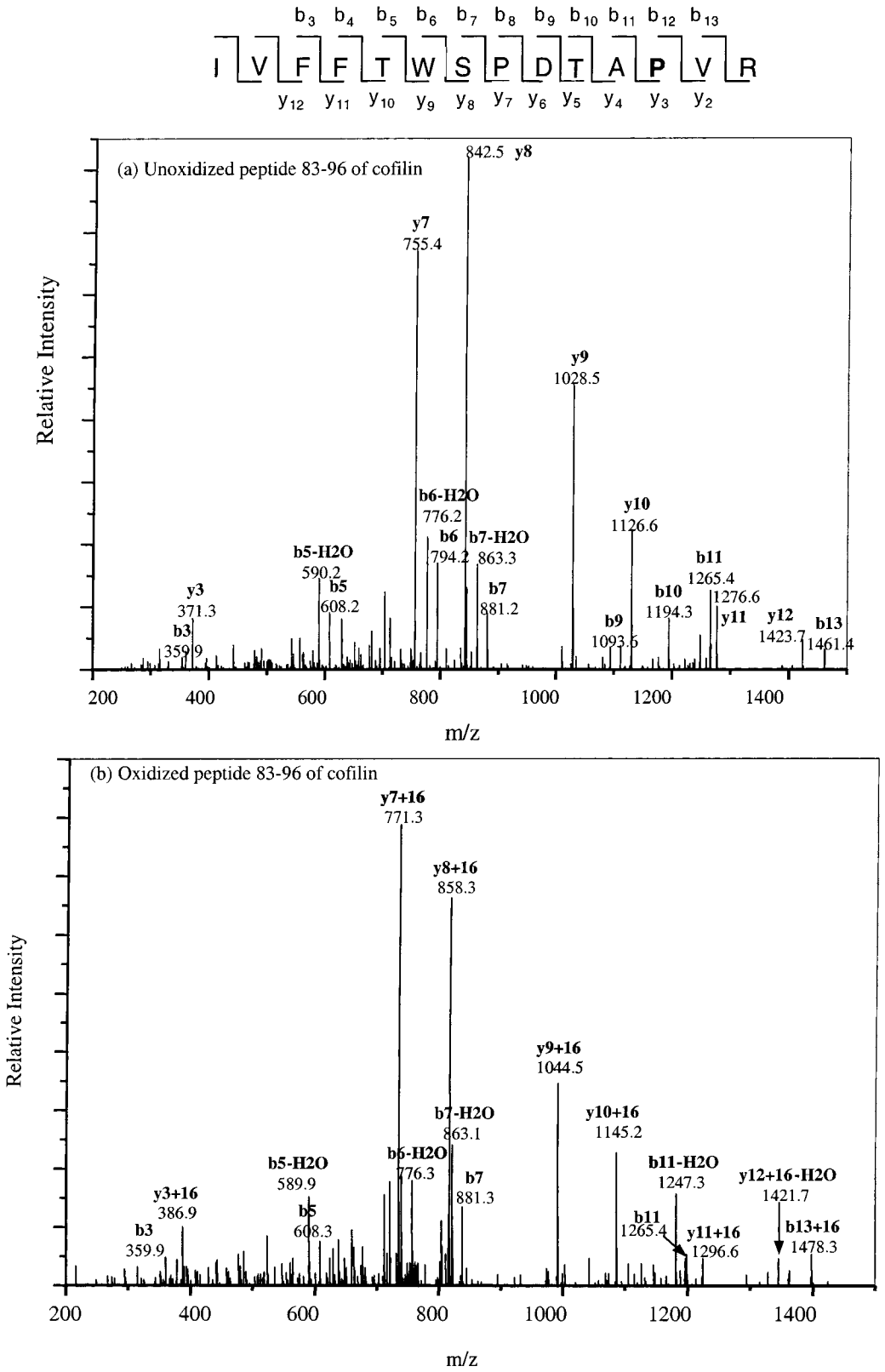

FIGURE 5. Collision-induced dissociation spectrum used to identify the modification site for peptide 83−96 of cofilin.

molecules is probed. First, the rate of the loss of the unmodified fraction is examined, emphasizing the disappearance of biologically intact material. Second, the total dose is limited. Third, the observation of first-order kinetics in the loss of the unmodified fraction ensures that dose-dependent changes in reactivity are not induced by the oxidations. These safeguards are the hallmark of all footprinting approaches, which depend on the covalent modification or cleavage of macromolecules to probe the structure (Figure 7).[40,45−47,52] It must be emphasized

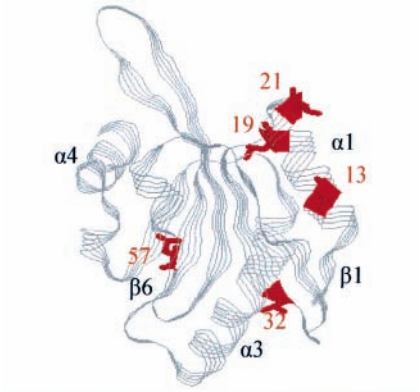

Residue	Rate (s^{-1})	Solvent Accessible Area ($Å^2$)
Leu-19	-	0.2
Leu-57	-	0.8
Leu-32	0.23 ± 0.03	7.8
Leu-13	0.51 ± 0.04	51
Leu-21	0.95 ± 0.18	120

FIGURE 6. Oxidation rates and solvent accessibilities of selected leucine residues in cofilin.

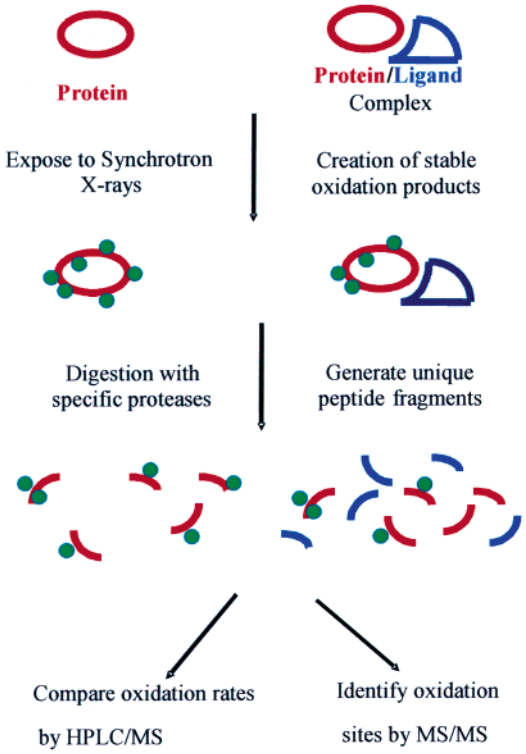

FIGURE 7. Overall method of protein footprinting using synchrotron radiolysis and mass spectrometry. The example emphasizes the protection formed in the interface of a protein/protein complex; however, the comparison could be for any two functional states of the protein of interest.

that footprinting provides only "local" information about the reactivity of the side chain probes. Allosteric changes in conformation induced by ligand binding can also give rise to either protections (decreases in side chain reactivity) or enhancements (increases in reactivity) depending on the nature of the induced conformational changes. This must be carefully considered when interpreting data from these experiments, and examples of each of these are provided in this Account. This caution is especially pertinent in the examination of ligand binding, where the formation of a binding interface gives rise to protections; however, confirmation of the interface must be sought through additional biochemical, structural, or genetic studies.

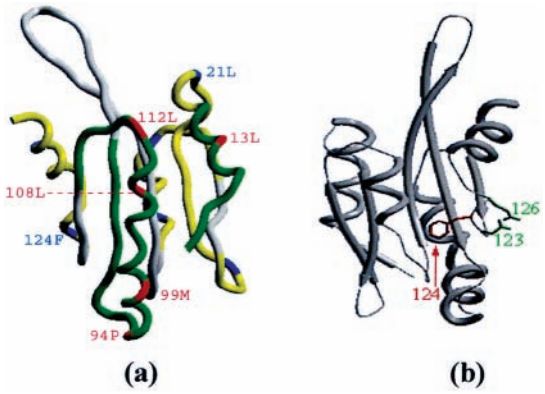

FIGURE 8. Footprinting results of cofilin bound to actin: (a) peptides that exhibit protection upon actin binding colored in green (probes in red), and peptides with unchanged reactivity colored in yellow (probes in blue); (b) the structure of cofilin rotated 90° from the orientation in panel a. The side chain of Phe-124 indicated not to be protected upon actin binding (see panel a), points in an opposite direction to residues Asp-123 and Asp-126, which are indicated by mutagenesis to contribute to cofilin−actin binding.

Actin Binding Sites on Cofilin

Despite considerable effort over the past decade, the crystal structure of the cofilin/actin complex is not available. We have used footprinting to probe the residues within the interface. Eleven peptides were found to be oxidized for both cofilin and its actin complex. The rate of oxidation was found to be reduced within cofilin for five of the eleven peptides upon actin binding, while for the other six cofilin peptides, there was no change in reactivity.[45] Specifically, cofilin peptides corresponding to residues 4−20, 10−17, 83−96, 91−105, and 106−117 showed reactivity decreases averaging 80% upon complex formation. MS/MS demonstrated that residues 13L, 94P, 99M, and 108L and 112L are the relevant probes. These results suggested an "actin binding surface" that includes Pro-94 just prior to the α3 helix, the long α3 helix (residues 99M, 108L, and 112L), and the N-terminal segments that encompass Leu-13 (Figure 8a). In contrast, a number of modified residues, such as Leu-21, Phe-124, and Leu-133 and His-143, are not protected and thus are not predicted to participate in the binding interface. These observations provide a model for the cofilin−actin interface, which is consistent with mutagenesis and biochemical studies indicating that the G-actin binding surface of cofilin includes the N-terminus (helix α1 and strand β1), the long central α3 helix, and the loop connecting strand β6 and

helix α4 (Figure 5).[53,54] Phe-124 was not protected upon actin binding, yet mutations of adjacent residues Asp-123 and Glu-126 have been shown to attenuate the actin/cofilin interaction.[45,53] Figure 8b shows clearly that Phe-124 is pointed away from the proposed interface while Asp-123 and Glu-126 project toward the predicted interface. Thus, the radiolytic footprinting and mutagenesis results are fully complementary.

The Solution Structure of Isolated G-Actin Is Divalent Cation Dependent

The capability of footprinting to reveal ligand-dependent changes is dramatically illustrated by examining actin monomer structure as a function of divalent cation binding. Twenty-eight peptides of actin (~90% sequence coverage), containing fifty-eight distinct probe sites, were examined to monitor divalent cation dependent structural variations of G-actin. The solvent accessibilities of the probe sites in solution, as measured by the reactivity of the peptides derived from the Ca^{2+}-G-actin and Mg^{2+}-G-actin complexes with GS1, were consistent with available crystallographic data.[18,21] Because most of the peptides monitored for isolated Ca-G-actin outside the GS1 contact interface have indistinguishable reactivity to those in the actin/GS1 complexes, the local structure of Ca-G-actin in solution is similar to the actin structure within the GS1 complexes. In contrast to the corresponding residues in Ca-G-actin, residues 40H, 44M, 47M, 53Y, 67L, and 69Y in subdomain 2, residues 200F−202T and 243P in subdomain 4, and residues 362Y, 367P, 371H, 374C, and 375F in the C-terminal region had reduced reactivity for isolated Mg-G-actin. A consistent structural explanation for many of these changes would be a narrower cleft between subdomains 2 and 4 and a C-terminus more closely packed onto subdomain 1 in Mg-G-actin (Figure 9). The observation of altered reactivity in the D-loop (40H, 44M, and 47M) in Mg-G-actin is consistent with the flexibility illustrated in the crystal structures of actin complexes, where the D-loop can have different secondary structures and orientations relative to subdomain 4.[16−21]

Many residues monitored in subdomains 1, 3, and 4 do not show appreciable differences in reactivity between Ca- and Mg-G-actins. These residues include the linker between subdomains 1 and 3, the putative H-loop, and many other segments (such as the N-terminus, helices or loops 84−93, 118−125, 316−326, and 222−243). These results suggest that Ca^{2+}- and Mg^{2+}-G-actin share similar conformations within many regions of subdomains 1, 3, and 4.[51]

Structure of Actin Filaments

The solution structures of Ca- and Mg-G-actin mapped above show that probes in the cleft between subdomains 2 and 4 and in the C-terminus, such as 44M, 47M, 202T, 243P, and 375F, are protected in the Mg^{2+} state. These residues, as well as residues 322P, 325M, 166H, 169Y, 110L, 112P, and 269M, are located in intermolecular contacts in the helical model of F-actin (Figure 2b). The protections

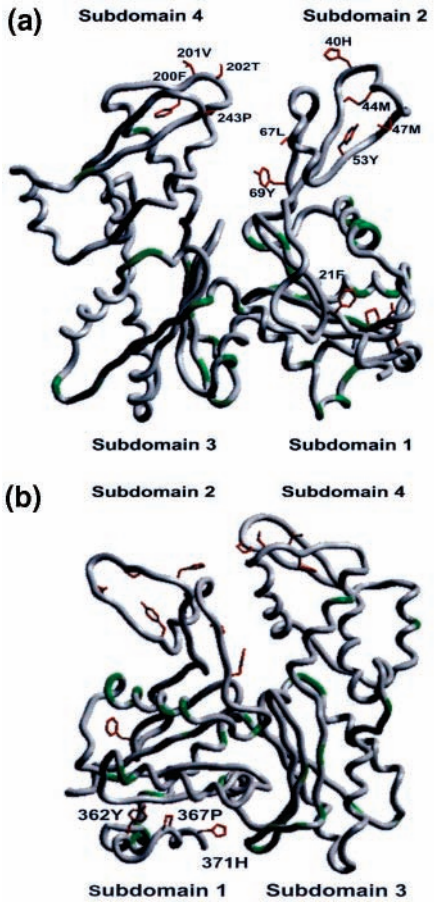

FIGURE 9. Actin monomer structures showing that the structure of G-actin in solution is divalent cation dependent. The backbone trace is from the crystal structure of G-actin in the G-actin/DNase I complex with the DNase I removed.[17] Colored in green are the backbones of the residues that are identified within peptides showing the same rate of reactivity for Ca-G-actin and Mg-G-actin. Colored in red are the side chains of the residues from peptides showing less reactivity in Mg-G-actin compared to Ca-G-actin. Probes that are involved in the conformational variation within subdomains 2 and 4 are highlighted in panel a and those within the C-terminus in panel b. Residues 374C and 375F were also monitored, although they are invisible in the crystal structure.

observed in Mg-G-actin possibly suggest that structural changes at subdomain 2 and the C-terminus contribute to the well-known ease of Mg-G-actin polymerization. As Mg-G-actin polymerizes to Mg-F-actin, residues 44M, 47M, 110L, 112P, 202T, 243P, and 375F are observed to be further protected, supporting the predictions of the helical model.[22] However, residues 322P and 325M in Mg−F-actin were observed to be as accessible to solvent as in G-actin, and residues 166Y, 169Y, and 269M were observed to be more exposed. These results suggest that the transition from Mg-G-actin to Mg-F-actin leads to additional protections on subdomain 2 and the C-terminus, together with other structural changes monitored in the H-loop and residues 157−178. The observation of increased exposure, particularly for the H-loop residue 269M, is in disagreement with the helical model. Discrepancies with the helical model were also observed for some residues in the small domain such as 69Y, 73H, 79W, 82M,

119M, and 123M, which are observed to be more protected than what is predicted by the helical model. Many residues within the large domain, such as 322P, 325M, 227M, and 236L, were observed to show no change in solvent accessibility relative to the actin monomer, although the helical model suggests protection for residues 322P and 325M. On the other hand, many probes in the large domain, like 305M-307P, 332P and 333P, which are located in the outer face of actin in the helical model, behave as predicted. Overall, the data indicate that in Mg−F-actin, the actin subunits are oriented such that the small domain is more tightly packed to the axis of filaments and that the large domain is less tightly packed than predicted by the helical model.

In the ribbon model, subdomains 1 and 2 are near the center of the ribbon and the subdomains 3 and 4 interface is near the exterior. This orientation of actin subunits seems to be plausible on the basis of the protections we observed in the small and large domains of actin. However, residues 69Y, 73H, 79W, 82M, 119M, and 123M, which are clearly protected in F-actin relative to G-actin, are predicted to be as exposed in F-actin as in G-actin for the ribbon model. Moreover, the observation of a more exposed H-plug in F-actin is also the opposite of what is predicted by the ribbon model.[27] Thus, the data suggest a modestly altered helical model is preferred over the ribbon model.

Concluding Remarks

Radiolytic protein footprinting coupled to mass spectrometry has been developed over the last several years and has matured into a viable approach for analyzing protein structure and dynamics. In this Account, we review the application of these methods to identify the interactions between actin and actin binding proteins, the solution structures of isolated G-actins, and the structural transitions of actin as a function of polymerization. These methods have opened new opportunities to conduct actin cytoskeleton research, where examining the structures of proteins or their complexes suffers intrinsic limitations. In the future, we envision experiments that would examine the time-resolved dynamics of actin assembly and disassembly using footprinting. Moreover, since these techniques can be applied under various solution conditions without intrinsic limitations, a wide range of physiologically relevant experiments are possible with complex multicomponent systems.

This work is supported by the NIH through Grants P41-EB-01979, P01-GM-66311, R33-CA-84173, R01-GM-53807, and R01-AR-22031.

References

(1) Pollard, T. D.; Blanchoin, L.; Mullins, R. D. Molecular mechanism controlling actin filament dynamics in nonmuscle cells. *Annu. Rev. Biophys. Biomol. Struct.* **2000**, *29*, 545−576.
(2) Higgs, H. N.; Pollard, T. D. Regulation of actin filament network formation through ARP2/3 complex: activation by a diverse array of proteins. *Annu Rev Biochem.* **2001**, *70*, 649−676.
(3) Cassimeris, L.; Safer, D.; Nachmias, V. T.; Zigmond, S. H. Thymosin β4 sequesters the majority of G-actin in resting human polymorphonuclear leukocytes. *J. Cell Biol.* **1992**, *119*, 1261−1270.
(4) Pantaloni, D.; Carlier, M. F. How profilin promotes actin filament assembly in the presence of thymosin β4. *Cell* **1993**, *75*, 1007−1014.
(5) Mahoney, N. M.; Janmey, P. A.; Almo, S. C. Structure of the profilin-poly-L-proline complex involved in morphogenesis and cytoskeletal regulation. *Nat. Struct. Biol.* **1997**, *4*, 953−960.
(6) Cooper, J. A.; Schafer, D. A. Control of actin assembly and disassembly at filament ends. *Curr. Opin. Cell Biol.* **2000**, *12*, 97−103.
(7) Burtnick, L. D.; Koepf, E. K.; Grimes, J.; Jones, E. Y.; Stuart, D. I.; McLaughlin, P. J.; Robinson, R. C. The crystal structure of plasma gelsolin: implications for actin severing, capping, and nucleation. *Cell* **1997**, *90*, 661−670.
(8) Bamburg, J. R. Protein of the ADF/cofilin family: essential regulators of actin dynamics. *Annu. Rev. Cell Dev. Biol.* **1999**, *15*, 185−230.
(9) Mejean, C.; Hue, H. K.; Pons, F.; Roustan, C.; Benyamin, Y. Cation binding sites of actin: a structural relationship between antigenic epitopes and cation exchange. *Biochem. Biophys. Res. Commun.* **1988**, *152*, 368−375.
(10) Estes, J. E.; Selden, L. A.; Kinosian, H. J.; Gershman, L. C. Tightly bound divalent cation of actin. *J. Muscle Res. Cell Motil.* **1992**, *13*, 272−284.
(11) Slosarek, G.; Heintz, D.; Kalbitzer, H. S. Mobile segments in rabbit skeletal muscle F-actin detected by 1H nuclear magnetic resonance spectroscopy. *FEBS Lett.* **1994**, *351*, 405−410.
(12) Strzelecka-Golaszewska, H.; Wozniak, A.; Hult, T.; Lindberg, U. Effect of the type of divalent cation, Ca^{2+} or Mg^{2+}, bound at the high-affinity site and of the ionic composition of the solution on the structure of F-actin. *Biochem. J.* **1996**, *316*, 713−721.
(13) Nyitrai, M.; Hild, G.; Belagyi, J.; Somogyi, B. Spectroscopic study of conformation changes in subdomain 1 of G-actin: influence of divalent cations. *Biophys. J.* **1997**, *73*, 2023−2032.
(14) Moraczewska, J.; Wawro, B.; Seguro, K.; Strzelecka-Golaszewska, H. Divalent cation-, nucleotide- and polymerization-dependent changes in the conformation of subdomain 2 of actin. *Biophys. J.* **1999**, *77*, 373−385.
(15) Pollard, T. D. Actin. *Curr. Opin. Cell Biol.* **1990**, *2*, 33−40.
(16) Otterbein, L. R.; Craceffa, P.; Dominguez, R. The crystal structure of uncomplexed actin in the ADP state. *Science* **2001**, *293*, 708−711.
(17) Kabsch, W.; Mannherz, H. G.; Suck, D.; Pai, E. F.; Holmes, K. C. Atomic structure of the actin:DNase I complex. *Nature* **1990**, *347*, 37−44.
(18) McLaughlin, P. J.; Gooch, J. T.; Mannherz, H.-G.; Weeds, A. G. Structure of gelsolin segment 1-actin complex and the mechanism of filament severing. *Nature* **1993**, *364*, 685−692.
(19) Schutt, C. E.; Myslik, J. C.; Rozycki, M. D.; Goonesekere, N. C. W.; Lindberg, U. The structure of crystalline profilin: β-actin. *Nature* **1993**, *365*, 810−816.
(20) Head, J. F.; Swamy, N.; Ray, R. Crystal structure of the complex between actin and human vitamin D-binding protein at 2.5 Å resolution. *Biochemistry* **2002**, *41*, 9015−9020.
(21) Vorobiev, S.; Strokopytov, S.; Drubin, D. G.; Frieden, C.; Ono, S.; Condeelis, J.; Rubenstein, P. A.; Almo, S. C. The Structure of Non-Vertebrate Actin: Implications for the ATP Hydrolytic Mechanism. *Proc. Natl. Acad. Sci. U.S.A.* **2003**, *100*, 5760−5765.
(22) Holmes, K. C.; Popp, D.; Gebhard, W.; Kabsch, W. Atomic model of the actin filament. *Nature* **1990**, *347*, 44−49.
(23) Lorenz, M.; Popp, D.; Holmes, K. C. Refinement of the F-actin model against X-ray fiber diffraction data by the use of a directed mutation algorithm. *J. Mol. Biol.* **1993**, *234*, 826−836.
(24) Tirion, M. M.; ben-Avraham, D.; Lorenz, M.; Holmes, K. C. Normal modes as refinement parameters for the F-actin model. *Biophys. J.* **1995**, *68*, 5−12.
(25) Egelman, E. H.; Orlova, A.; Mcgough, A. Only one F-actin model. *Nat. Struct. Biol.* **1997**, *4*, 683−684.
(26) Orlava, A.; Egelman, E. H. A conformational change in the actin subunit can change the flexibility of the actin filament. *J. Mol. Biol.* **1993**, *232*, 334−341.
(27) Schutt, C. E.; Rizycki, M. D.; Chik, J. K.; Lindberg, U. A discourse on modeling F-actin. *J. Struct. Biol.* **1995**, *115*, 186−198.
(28) Klassen, N. V. In *Radiation Chemistry Principles & Applications*; Farhatazis, Rodgers, M. A., Eds.; VCH: Texas, 1987; pp 29−61.
(29) Sclavi, B.; Sullivan, M.; Chance, M. R.; Brenowitz, M.; Woodson, S. A. RNA Folding at Millisecond Intervals by Synchrotron Hydroxyl Radical Footprinting. *Science* **1998**, *279*, 1940−1943.
(30) Sclavi, B.; Woodson, S.; Sullivan, M.; Chance, M. R.; Brenowitz, M. Following the Folding of RNA with Time-Resolved Synchroton X-ray Footprinting. *Methods Enzymol.* **1998**, *295*, 379−402.
(31) Maleknia, S. D.; Ralston, C. Y.; Brenowitz, M.; Downard, K. M.; Chance, M. R. Determination of Macromolecular Folding and Structure by Synchrotron X-ray Radiolysis Techniques. *Anal. Biochem.* **2001**, *289*, 103−115.

(32) Ralston, C. Y.; Scalvi, B.; Sullivan, M.; Deras, M. L.; Woodson, S. A.; Chance, M. R. Time-resolved synchrotron X-ray footprinting and its application to RNA folding. *Methods Enzymol.* **2000**, *317*, 353−368.
(33) Garrison, W. M. Reaction Mechanisms in the Radiolysis of Peptides, Polypeptides, and Proteins. *Chem. Rev.* **1987**, *87*, 381−398.
(34) Stadtman, E. R.; Berlett, B. S. Reactive oxygen-mediated protein oxidation in aging and disease. *Drug. Metab. Rev.* **1998**, *30*, 225−243.
(35) Hawkins, C. L.; Davies, M. J. Generation and propagation of radical reactions on proteins. *Biochem. Biophys Acta.* **2001**, *1504*, 196−219.
(36) Maleknia, S. D.; Brenowitz, M.; Chance, M. R. Millisecond radiolytic modification of peptides by synchrotron X-rays identified by mass spectrometry. *Anal.Chem.* **1999**, *71*, 3965−3973.
(37) Aebersold, R.; Mann, M. Mass spectrometry-based proteomics. *Nature* **2003**, *422*, 198−207.
(38) Ferguson, P. L.; Smith, R. G. Proteome analysis by mass spectrometry. *Annu. Rev. Biophys. Biomol. Struct.* **2003**, *32*, 399−424.
(39) Xu, G.; Chance, M. R. Radiolytic Modification of Basic Amino Acid Residues in Peptides: New Probes for Examining Protein−Protein Interactions. *Anal. Chem.* **2003**, *75*, 6995−7007.
(40) Kiselar, J. G.; Maleknia, S.; Sullivan, M.; Downard, K.; Chance, M. R. Hydroxyl Radical Probe of Protein Surfaces Using Synchrotron X-ray Radiolysis and Mass Spectrometry. *Int. J. Rad. Biol.* **2002**, *78*, 101−114.
(41) Chance, M. R. Unfolding of Apomyoglobin Examined by Synchrotron Footprinting. *Biochem. Biophys. Res. Commun.* **2001**, *287*, 614−621.
(42) Kiselar, J. G.; Janmey, P.; Almo, S. C.; Chance, M. R. Visualizing the Ca^{2+} Dependent Activation of Gelsolin by Using Synchrotron Footprinting. *Proc. Natl. Acad. Sci. U.S.A.* **2003**, *100*, 3942−3947.
(43) Liu, R.; Guan, J.-Q.; Zak, O.; Aisen, P.; Chance, M. R. Structural Reorganization of Transferrin C-lobe and Transferrin Receptor Upon Complex Formation: C-lobe Binds to the Receptor Helical Domain. *Biochemistry* **2003**, *42*, 12447−12454.
(44) Rashidzadeh, H.; Khrapunov, S.; Chance, M. R.; Brenowitz, M. Solution structure and interdomain interactions of the *Saccharomyces cerevisiae* "TATA binding protein" (TBP) probed by radiolytic protein footprinting. *Biochemistry* **2003**, *42*, 3655−3665.
(45) Guan, J.-Q.; Vorobiev, S.; Almo, S. C.; Chance, M. R. Mapping the G-actin binding surface of cofilin using synchrotron protein footprinting. *Biochemistry* **2002**, *41*, 5765−5775.
(46) Guan, J.-Q.; Chance, M. R. Footprinting methods to examine the structure and dynamics of proteins. *Encycl. Mol. Cell Biol. Mol. Med.* **2004**, in press
(47) Takamoto, K. G.; Chance, M. R. Footprinting Methods to Examine the Structure and Dynamics of Nucleic Acids. *Encycl. Mol. Cell Biol. Mol. Med.* **2004**, in press
(48) Goldsmith, S. C.; Guan, J.-Q.; Almo, S. C.; Chance, M. R. Synchrotron protein footprinting: a technique to investigate protein−protein interactions. *J. Biomol. Struct. Dyn.* **2001**, *19*, 405−418.
(49) Galas, D.; Schmitz, A. DNase footprinting: a simple method for the detection of protein-DNA binding specificity. *Nucleic Acids Res.* **1978**, *5*, 3157−3170.
(50) Fedorov, A. A.; Lappalainen, P.; Fedorov, E. V.; Drubin, D. G.; Almo, S. C. Structure determination of yeast cofilin. *Nat. Struct. Biol.* **1997**, *4*, 366−369.
(51) Guan, J.-Q.; Almo, S. C.; Reisler, E.; Chance, M. R. Structural reorganization of proteins revealed by radiolysis and mass spectrometry: G-actin solution structure is divalent cation dependent. *Biochemistry* **2003**, *42*, 11992−12000.
(52) Kiselar, J. G.; Janmey, P.; Almo, S. C.; Chance, M. R. Structural analysis of gelsolin using synchrotron protein footprinting. *Mol. Cell. Proteomics* **2003**, *2*, 1120−1132.
(53) Lappalainen, P.; Fedorov, E. V.; Fedorov, A. A.; Almo, S. C.; Drubin, D. G. Essential functions and actin-binding surfaces of yeast cofilin revealed by systematic mutagenesis. *EMBO J.* **1997**, *16*, 5520−5530.
(54) Moriyama, K.; Yahara, I. Two activities of cofilin, severing and accelerating directional depolymerization of actin filaments, are affected differentially by mutations around the actin-binding helix. *EMBO J.* **1999**, *18*, 6752−6761.

AR0302235